Bloch lines in thin films with perpendicular magnetic anisotropy and intermediate quality factor

Journal of Physics: Conference Series **1389** (2019) 012002 doi:10.1088/1742-6596/1389/1/012002

Bloch lines in thin films with perpendicular magnetic anisotropy and intermediate quality factor

I M Izmozherov[1,2], V V Zverev [1,2] and Erlan Zh. Baykenov[2]

[1] Institute of metal physics UB RAS, 620990, Ekaterinburg, Russia
[2] Ural Federal University, 620002, Ekaterinburg, Russia

E-mail: izmozherov@imp.uran.ru

Abstract. Bloch lines (BLs) are linear topological defects of magnetic domain walls structure, studied well for bubble domain materials. We investigate its structure and role in magnetization reversal for thin ferromagnetic films with perpendicular magnetic anisotropy and intermediate quality factor. We observe vertical BLs with Bloch points and U-shaped structures with vertical and horizontal parts in three-dimensional micromagnetic simulations for $Q = 0.34$. Also we suggest analytical model functions, describing 3D magnetization distribution in domain walls with BLs.

1. Introduction

The domain structure (DS) of ferromagnetic thin films impacts significantly on macroscopic properties (hysteresis, magnetostriction, etc.). The study of DS in external fields is interesting both for applications as physical base for data storage devices [1] and for fundamental research, since DS is an example of an open system with complex dynamics and excitation of internal degrees of freedom. In particular, structural elements with non-trivial topological charge can be observed on domain walls (DWs). They are classified as linear and point defects (solitons) of magnetization vector field: Bloch lines (BLs) and Bloch points (BPs). In the simplest case analytical solution for one BL on Bloch-type DW, elongated along the x-axis in two-dimensional ferromagnetic media with quality factor $Q = K_u/2\pi M_s^2$ is [2] where K_u is uniaxial anisatropy constant and M_s is saturation magnetzation:

$$\Phi(x) = 2\arctan\left(\exp\left(\frac{x}{\Lambda_0}\right)\right), \qquad \Theta(y) = 2\arctan\left(\exp\left(\frac{y}{\delta_0}\right)\right) \tag{1}$$

Here Φ and Θ are azimuthal and polar angles for magnetization, and Λ_0 , δ_0 are BL and DW width parameters respectively. Schematic rerpresentation of such magnetization distribution is shown in the figure 1. However, films with the perpendicular magnetic anisotropy (PMA) and $0.1 < Q < 1$ have more complex BL structures which cannot be obtained just by translation of 2D distribution in the figure 1 in z-axis direction. There are several arguments for this. Firstly, DWs has a vortex structure [3], which is associated with the competition of the anisotropic and magnetostatic energy contributions. As a result, the DW has the Bloch type in the bulk and the Neel type near surfuces. This reduces the density of magnetostatic energy, when Neel caps

has opposite reversal directions. Due to these reasons BLs are not strictly vertical. They do not reach film surfaces, being itself the part of Neel DW, and consist of two fragments, with opposite chirality, separated by a BP.

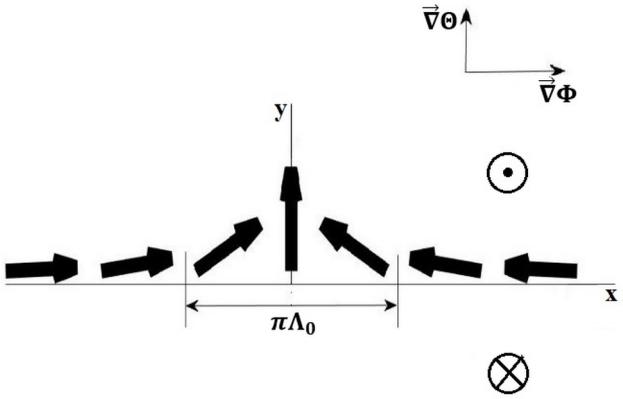

Figure 1. Schematic representation of vertical Bloch line structure in 2D-model.

These BL structures have been observed in micromagnetic simulations in the DS in a 200 nm thick film with Co (0001) material parameters [4]. We performed micromagnetic simulations using the *mumax*^{3} micromagnetic framework [5]. Here we discuss the results of magnetization reversal simulations for in-plane (IP), out-of-plane (OP) and intermediate (IM) DC magnetic field orientations. We focus on the BL transformations, which accompany DS transitions.

Also we suggest a 3D model distribution describing the magnetization in BLs, containing BPs, and prove its consistency by direct comparison with the distributions obtained in simulations, as well as calculating the the skyrmion number. To exclude misunderstanding in next chapters we always will use term "simulations" speaking about micromagnetics, and "model" speaking about analytical distribution.

2. Micromagnetic simulations

2.1. Problem definition

Micromagnetic simulations were carried out for the PMA sample with sizes: $L_x = L_y = 1024$ nm, $L_z = 200$ nm. Magnetic patterns were found by the numerical minimization of the total energy on the rectangular mesh using steepest descent method with adaptive step length variation. The cell sizes where equal: $l_x = l_y = 4$ mn, $l_z = 3.125$ nm. The energy functional for a normalized magnetization $\mathbf{m}(x, y, z)$ is defined as follows:

$$\begin{aligned} E &= \int_V d^3r(w_m + w_z + w_e + w_a), \\ w_m &= -\frac{1}{2}M_s(\mathbf{mH}_m), \\ w_z &= -M_s(\mathbf{mH}), \\ w_e &= A\left[\left(\frac{\partial \mathbf{m}}{\partial x}\right)^2 + \left(\frac{\partial \mathbf{m}}{\partial y}\right)^2 + \left(\frac{\partial \mathbf{m}}{\partial z}\right)^2\right], \\ w_a &= -K_1(\mathbf{km})^2 - K_2(\mathbf{km})^4 \end{aligned} \tag{2}$$

Here M_s is the saturation magnetization, $\mathbf{H}_m$ is the demagnetizing field, and K_1, K_2 are the anisotropy constants, $\mathbf{k}$ is a unit vector in the anisotropy axis direction ($\mathbf{k}$ is normal to the film surfices), A is the exchange constant and $\mathbf{H}$ is the external DC magnetic field. Numerical values of material parameters corresponds are: $M_s = 1435$ G, $A = 3.01 \cdot 10^6$ erg/cm, $K_1 = 4.46 \cdot 10^6$ erg/cm^3, $K_2 = 1.5 \cdot 10^6$ erg/cm^3 [5]. In *xy*-plane (parallel to film plane) periodic boundary conditions are defined: $\mathbf{m}|_{x=0} = \mathbf{m}|_{x=L_x}$, $\mathbf{m}|_{y=0} = \mathbf{m}|_{y=L_y}$. Special algorithms, based on numeric calculations of topological invariants, have been created for BL visualization.

2.2. Domain structure for zero extrinsic field and hysteresis loops simulations
An example of DS visualization for the case $\mathbf{H} = 0$ is shown in the figure 2. Starting from a random magnetization distribution we have obtained a fragment of labyrinth pattern. Vertical BLs with opposite chiralities, containing BPs with different signs of a topological charge, are in the DW in pairs (figure 2a). Specific cross sections of the magnetization distribution are shown in the figure 2b, figure 2c. The positions of the BLs are visible in sections I and II. It can be seen that the chiralities of the same BL are different in different sections, which is due to the presence of a BP. As it was discussed earlier, BLs do not reach film surfaces (figure 2a).

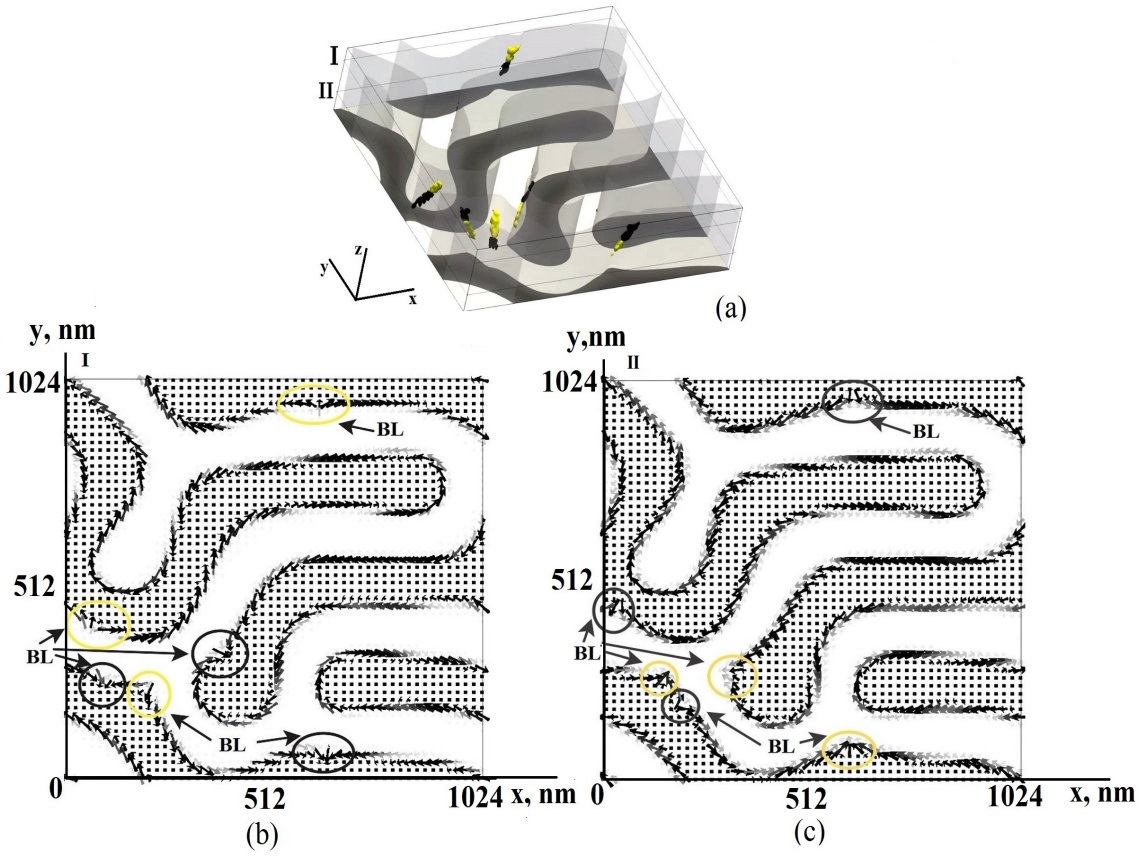

Figure 2. (a) The DS for $\mathbf{H} = 0$. Semiopaque surfaces denote DW centers ($m_z = 0$). Light (yellow) and black contours on DWs corresponds to BLs parts with opposite chiralities, connected by BPs (do not shown). Light and dark areas on bottom surface corresponds to domains with $m_z = \pm 1$ correspondingly. (b),(c) Magnetization distributions in the sections I and II.

Next, we turn on the external magnetic field and simulate the rotations of the magnetization for different orientations of $\mathbf{H}$. For each value of the field we minimize the energy functional.

We can observe DS transformations through three types of patterns: stripe domains, cylindric domains and the uniform magnetization. These transitions are accompanied by changes in the structure of the BLs. For the case of the IP field, stripe domains are stable. When field decreases

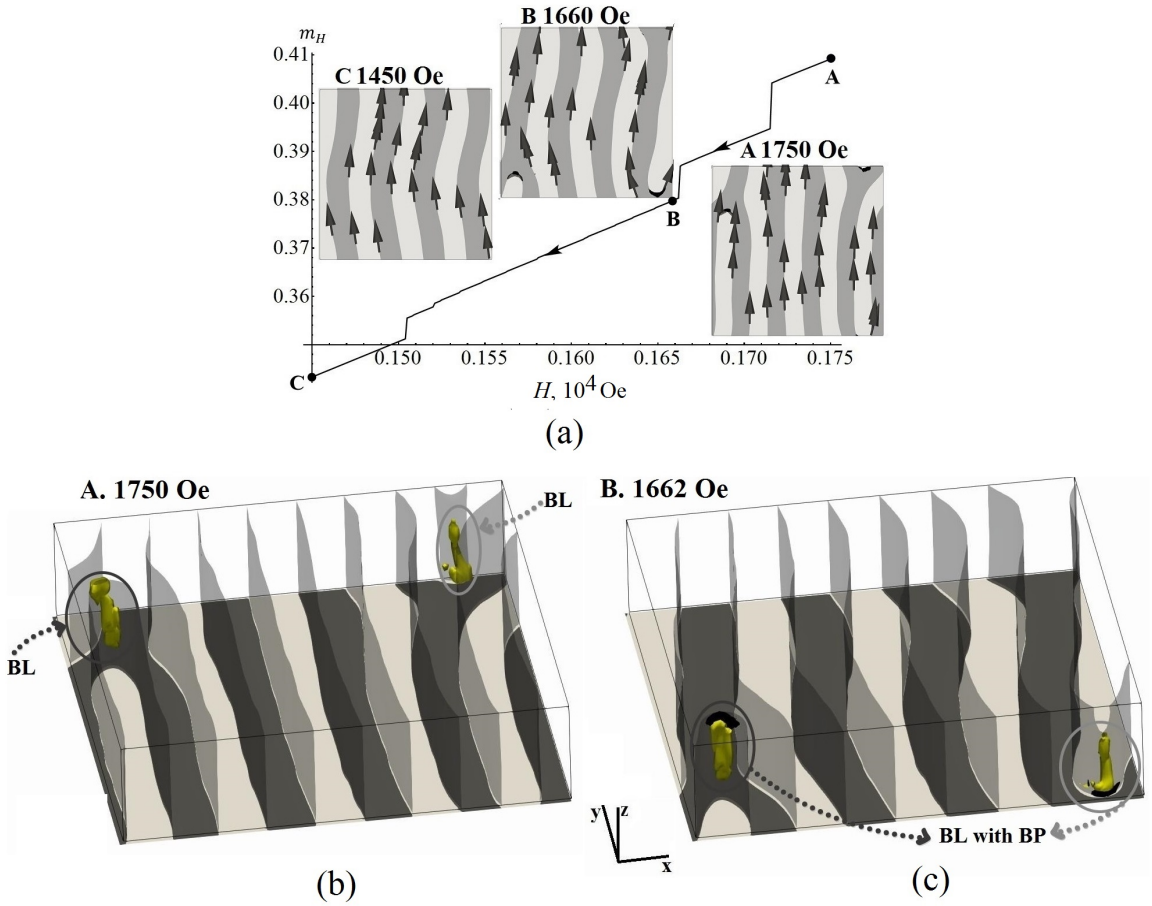

Figure 3. (a) Normalized magnetization projection on the field direction ($m_H = \frac{M_H}{M_s}$ and M_s is saturation magnetization) vs external field, for in-plane orientation. DS for points A,B,C are presented on inserts. Dark areas on DWs corresponds to BL positions (b) and (c) DS for points A and B correspondingly. Legend is similar to that in the figure 2a.

from saturation, one can observe the emergence and growth of the BL, containing BP. The BLs are located on the "heads" of the interrupted strip domains. On the first step (point A in the figure 3a) there are two BLs without BP which reach one of the film surfaces (see figure 3b). While the field value decreases, the BP and the segment of the BL with opposite chirality appear (see figure 3c). Then BLs with BPs annihilate, mediating the annihilation of magnetic dislocations (point C in the figure 3a). For the OP case, BL pairs with opposite chiralities can annihilate, if they are localized on one DW segment or on opposite points of cylindric domains (in the latter case, when reducing the domain diameter). Also BL pairs can born then two cylindric domains, with increasing diameters, collides each over. Examples of these processes are presented in the figure 4. Gray ellipse on the DS sketch for point A shows localization of BL pair ready for annihilation. White and black ellipses show regions of a future collision of cylindric domains. Corresponding ellipses on the sketch for the point B mark new BL pairs appearing due to these collisions.

For IM case there are field ranges of stability of stripe and cylindric domains. When field is

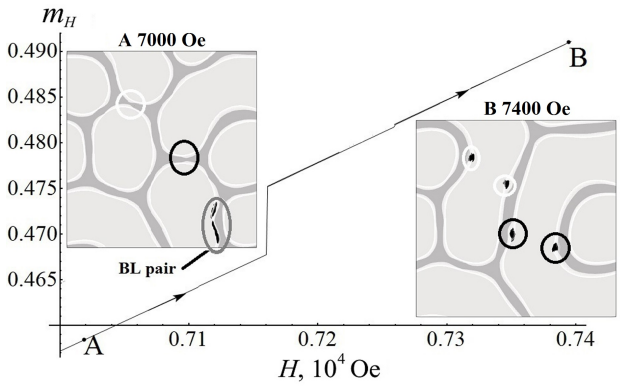

Figure 4. Normalized magnetization projection on the field direction ($m_H = \frac{M_H}{M_s}$ and M_s is saturation magnetization) vs external field, for the out-of-plane orientation. DSs for points A,B,C are presented on inserts. Dark areas on DWs corresponds to BL positions.

decreased from a saturation value, BL pairs appears on the opposite sides of cylindric domains involving IP mechanism discussed above (intrusion through surface). Most of these pairs then annihilate on cylindric domains involving OP mechanism. Transitions from cylindric to stripe domains occur while field is increasing in contrary direction. It can be mediated by new U-shaped BL-type structure, containing horizontal and vertical parts. This structure is shown in the figure 5b,c. Such structures are localized on cylindric domains (see figure 5b) and disappear with transitions to stripe domains in the part of the sample. Others may still exist on cylindric domains, as well as vertical BL pairs (see figure 5a).

3. Model function for a Bloch line

3.1. Description of a function

We present here an analytical model, describing three-dimensional structure of the Bloch line in material with intermediate quality factor $0.1 < Q < 1$ (for parameters used in simulations $Q = 0.34$). Analytical functions for polar Θ and azimuthal Φ angles (for magnetization) are defined in the region $G = [0 < x < x_{max}; 0 < y < y_{max}; 0 < z < z_{max}]$ (z-axis is normal to the film surfaces):

$$\Phi(x,z) = 2\arctan\left(\exp\left(\frac{x-\xi(z)}{\Lambda(z)}\right)\right) g(z) + \phi_s(x,z), \tag{3}$$

$$\Theta(x,y,z) = 2\arctan\left(\exp\left(\frac{y-f(x,z)}{\delta(z)}\right)\right)$$

These formulas are the generalization of (1) by the introduction of an auxiliary functions set.

(*i*) $f(x,z)$ is a function which defines the surface of the DW centers ($m_z = 0$). For the DS shown in the figure 2 it is usually curved rather than linear.

(*ii*) $\phi_s(x,z) = \arctan(\partial f(x,z)/\partial x)$ provides the tangential position of magnetization in a DW (Bloch DW) in each section $z = c$. To simplify the expression (3) in most cases one can assume $f(x,z)$ and $\phi_s(x,z)$ dependence only on x.

(*iii*) $\xi(z)$ is function of the BL "core" positions in different sections $z = c$. This function appearance is due to the fact, that BL is not strictly vertical, so line of BL "cores" is not normal to the film plane. In other words, you cannot just assume $\xi(z) \equiv 0$ as it is for model in the figure 1.

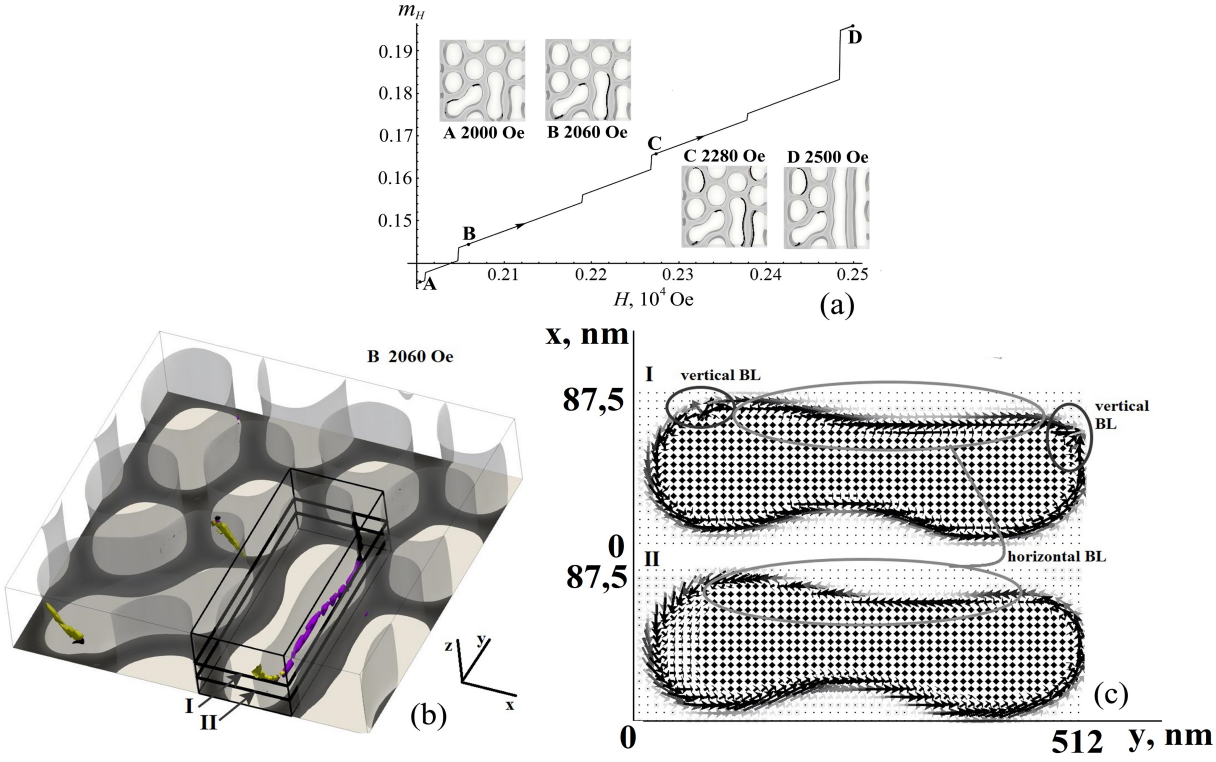

Figure 5. (a) Normalized magnetization projection on the field direction ($m_H = \frac{M_H}{M_s}$ and M_s is saturation magnetization) vs external field, for intermediate angle of field orientation. DSs in points A, B, C, D are presented on inserts. Dark areas on DWs corresponds to BL positions. (b) The DS for point B. Purple contour denotes horizontal BL section, other notations are similar to that in the figure 2a (c) Magnetization distribution in sections I and II for cylindric domain containing U-shaped BL structure.

(*iv*) $g(z) = 2\eta(z - z_{BP}) - 1$. Here z_{BP} is BP z-position and $\eta(z - z_{BP})$ is the Heaviside step function. This function provides the nonanalytical "switch" between rotation directions in BL (for $z > z_{BP}$ - $g(z) = 1$ and for $z < z_{BP}$ - $g(z) = -1$).

(*v*) $\delta(z)$ is a function of DW width parameters in different sections $z = c$. DW width should grow from the central plane $z = z_{max}/2$ to film surfaces due to the magnetic flux closure near film surfaces, which lowers magnetostatic energy density. Additional conditions for this function are:

$$\left.\frac{|y - f(x,z)|}{\delta(z)}\right|_{y=0} \gg 1; \qquad \left.\frac{y - f(x,z)}{\delta(z)}\right|_{y=y_{max}} \gg 1. \tag{4}$$

Applying (4) in (3), we can rewrite the conditions (4) in more clear way:

$$\Theta|_{y=0} \simeq 0, \qquad \Theta|_{y=y_{\max}} \simeq \pi. \tag{5}$$

Thus, it is just boundary conditions corresponding to the magnetization for neighboring domains.

(*vi*) $\Lambda(z)$ is a function of BL width parameters in different sections $z = c$. Here width should grow from $z = z_{BP}$ ($\Lambda(z_{BP} = 0)$) to $z = z_{max}$ and $z = 0$. This condition provide the existence

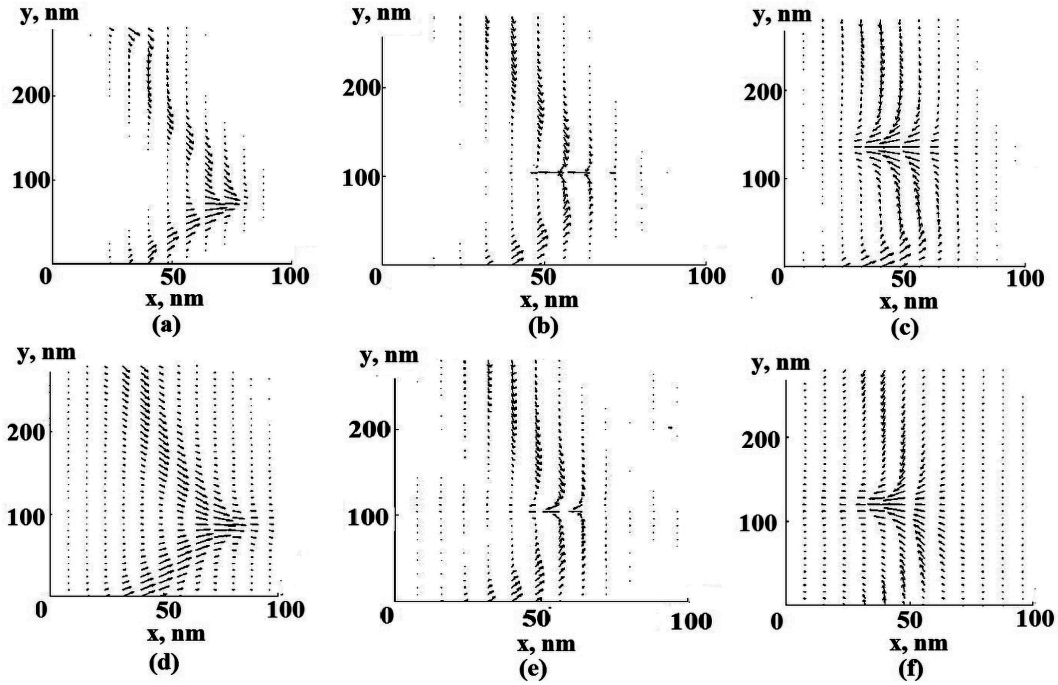

Figure 6. Comparative view of magnetization distributions in model (a,b,c) and simulation (d,e,f) in sections $z = 50$ nm (a,d), $z = 100$ nm (b,e) and $z = 150$ nm (c,f). Film thickness z_{max} = 200nm.

of BP as a point of singularity of magnetization field. Additionally, function must meet the conditions:

$$\frac{|x - \xi(0)|}{\Lambda(0)} \ll 1, \qquad \frac{|x - \xi(z_{max})|}{\Lambda(z_{max})} \ll 1. \tag{6}$$

Applying (6) in (3) and taking $g(z)$ definition into account we can write:

$$\Phi(x, 0) = -\frac{\pi}{2} + \phi_s(x, 0), \qquad \Phi(x, z_{max}) = \frac{\pi}{2} + \phi_s(x, z_{max}). \tag{7}$$

Therefore, this condition just states contrary Néel DW rotations on bottom and top surfaces. In the case, then the DW in region G has a reflective symmetry in the $x = x_{max}/2$ plane, it is reasonable to consider $\phi_s(x, 0) = \phi_s(x, z_{max}) = \phi_s(x)$. This set of functions allows to describe main features of the vertical BL magnetization distribution.

3.2. Model verification

Let us show that the suggested model meets topological constraints associated with the existence of BP in the region G. It means that the skyrmion number $\chi = \pm 1$, where χ is defined as a surface integral of gyrotropic vector density:

$$\chi = \frac{1}{4\pi} \oint\limits_G \mathbf{g} d\mathbf{s}, \qquad \mathbf{g} = [\nabla(\cos\Theta) \times \nabla\Phi] \ . \tag{8}$$

Firstly, we show that the integral values are equal to zero on the planes $y = 0, y = y_{max}$ due to the condition (5). Then using approximations (5) and (7), we separately calculate the

contributions of boundary planes to the value of the integral (8). χ_b, χ_t, χ_r, χ_f are contributions from $z = 0$, $z = z_{max}$, $x = 0$, $x = x_{max}$ correspondingly (surface orientations are taken as in the closed-surface integral (8)):

$$\chi_b = -\chi_t = \frac{1}{2\pi}(\phi_s(x_{max}) - \phi_s(0)), \qquad \chi_r = \chi_f = \frac{1}{2}. \tag{9}$$

Thus, the total value is $\chi = \chi_b + \chi_t + \chi_f + \chi_r = 1$ as it has to be for the positively charged BP situated in the region. Further, we directly compare results obtained by simulations and model calculations, approximating the auxiliary functions set as polynomials in least squares sense. Reference points for each function have been obtained from the simulation data taken from a simulation window subregion, containing the BL.

We base on these refer points to obtain Φ and Θ according to formulas (3). Magnetization vector components are $m_x = \cos\Phi\sin\Theta$, $m_y = \sin\Phi\sin\Theta$, $m_z = \cos\Theta$. Fig.6 shows direct comparison of model vs simulation results in three sections: $z = z_{max}/4$, $z_{max}/2$, $3z_{max}/4$. One can see qualitative agreement of modelled and simulated magnetization distributions. Relative deviations for magnetization componenets averaged over the BL containing area are $\Delta m_x/m_x \sim 0.04$, $\Delta m_y/m_y \sim 0.07$, $\Delta m_z/m_z \sim 0.02$.

4. Conclusions

Micromagnetic simulations allow us to obtain 3D visualizations for the domain structure of thin ferromagnetic film with perpendicular magnetic anisotropy. We show that without extrinsic DC field domain walls contain a small number of Bloch line pairs and each Bloch line contains Bloch point in its structure. Also we qualitatively investigate the scenarios of Bloch line transformations in in-plane, out-of-plane and intermediate angled DC extrinsic field which follows the domain structure transformations. In particular the process of the U-shaped Bloch line structure emergence which follows DS transformation from cylindric to stripe domains is described. Also the generalization of the isolated vertical Bloch line model is obtained for the thin films with intermediate quality factors. This model allows to consider the Bloch line with Bloch point in its structure and obtain the correct skyrmion number. Also the vortex structure of domain wall which the Bloch line mgnetization distribution can be considered. We can conclude that model (3) has a reasonable agreement with simulated results and can be used in further investigations.

Acknowledgments

The research was carried out within the state assignment of FASO of Russia (theme "Alloys" no. AAAA-A19-119070890020-3), and in the framework of the Russian Federation Government Resolution no. 211, contract no. 02.A03.21.0006.

Reference

[1] Bharati T, Ashutosh T 2017 *Vacuum* **146** 329-341
[2] Malozemoff A P, Slonchzewski J C 1979 *Magnetic Domain Walls in Bubble Materials. Advances in Materials and Device Research* (New York: Academic Press Inc.)
[3] Labrune M, Miltat J 1994 *J. Appl. Phys.* **75** 2156-2168
[4] Baykenov E Zh, Izmozherov I M, Zverev V V 2019 *Bulletin of the Russian Academy of Sciences Physics* **83** 809-811
[5] Vansteenkiste A, Leliaert J, Dvornik M, Helsen M, Garcia-Sanchez F, Van Waeyenberge B 2014 *AIP Advances* **4** 107133
[6] Naik R, Hameed S, Talagala P, Wenger L E 2002 *J. Appl. Phys.* **91** 7550-7552
[7] Pamyatnykh L A, Filippov B N, Agafonov L Y, Lysov M S 2017 *Scientific Reports* **7** 1-11
[8] Fallarino L, Hovorka O, Berger A 2016 *Phys. Rev. B.* **94** 1-13